Journal of Materials Chemistry C

ROYAL SOCIETY OF CHEMISTRY

PAPER

View Article Online
View Journal

Check for updates

Cite this: DOI: 10.1039/d5tc04488j

Mechanochromism of dinuclear aluminum-based triple-stranded helicates through crystalline-to-amorphous phase transition

Tomoya Umeki,[a] Ayano Tani,[a] Yuto Konishi,[a] Yusuke Ishigaki,[b] Takunori Harada,[c] Takumi Ehara,[d] Kiyoshi Miyata,[d] Ken Onda,[d] Yu Hoshino[ae] and Toshikazu Ono*[ae]

Received 23rd December 2025,
Accepted 27th March 2026

DOI: 10.1039/d5tc04488j

rsc.li/materials-c

This study explores the mechanochromic behavior of dinuclear aluminum-based triple-stranded helicates with various halogenated substituents. Mechanical grinding induces distinct color changes, with powder X-ray diffraction confirming phase transitions between crystalline and amorphous states. In the crystalline phase, the helicates adopt a more twisted conformation that limits π-conjugation, producing monomeric yellow emission. In contrast, in the amorphous phase, this twist relaxes and the π-conjugated system is extended, yielding orange emission. The original emission properties can be restored through solvent treatment, demonstrating the reversible nature of this mechanochromic behavior. These results demonstrate a mechanochromic mechanism governed by reversible torsion-angle changes and highlight aluminum-based helicates as promising responsive luminescent materials.

Introduction

Mechanochromism, the phenomenon in which molecules or materials exhibit visible color changes in response to mechanical stimuli, has attracted significant research interest owing to its promising applications in sensors, displays, and optical devices.[1–14] This phenomenon typically arises when external forces alter the crystal structure or intermolecular interactions within a material, leading to changes in electronic states and luminescence properties (Fig. 1(a)). Thus, mechanochromic materials, such as organic dyes and metal complexes that display color and emission changes in response to external stimuli such as grinding, stretching, and compression, are increasingly recognized as next-generation functional materials.[15–18]

Traditionally, most mechanochromic materials comprise complexes of precious metals, including platinum and gold.[19–26] Although these materials offer exceptional photophysical properties, the reliance on precious metals poses challenges owing to resource limitations, high costs, and environmental impact. To address these issues, research efforts have shifted toward alternative materials based on more abundant and cost-effective elements such as zinc and copper.[27–31] Among such elements, aluminum stands out as an earth-abundant and inexpensive metal ion, making it a promising candidate for sustainable material development. The most well-known example, AlQ_3 (tris(8-hydroxyquinoline)aluminum), has been

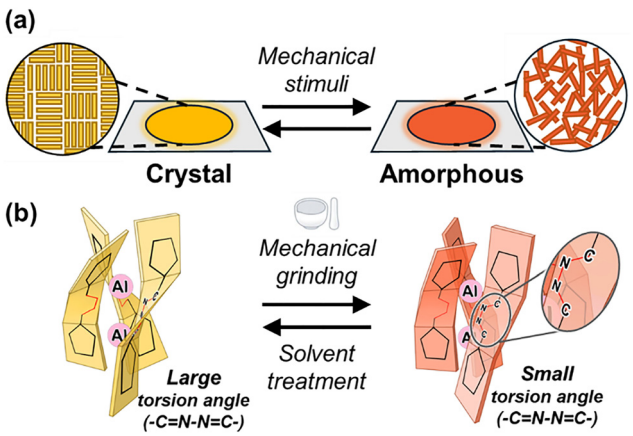

Fig. 1 (a) Mechanochromism induced by phase transitions between crystalline and amorphous states. (b) Schematic illustration of an aluminum-based dinuclear triple-stranded helicate (ALPHY), emphasizing that the mechanochromic response originates from changes in the ligand torsion angle of the helical structure (–C═N–N═C–) upon mechanical grinding and subsequent solvent-mediated recovery as the origin of the mechanochromic response.

[a] Department of Applied Chemistry, Graduate School of Engineering, Kyushu University, 744 Motooka, Nishi-ku, Fukuoka 819-0395, Japan. E-mail: tono@mail.cstm.kyushu-u.ac.jp
[b] Department of Chemistry, Faculty of Science, Hokkaido University, Sapporo 060-0810, Japan
[c] Faculty of Science and Technology, Graduate School of Engineering, Oita University, 700 Dannoharu, Oita City 870-1192, Japan
[d] Department of Chemistry, Faculty of Science, Kyushu University, 744 Motooka, Nishi-ku, Fukuoka, 819-0395, Japan
[e] Center for Molecular Systems (CMS), Kyushu University, 744 Motooka, Nishi-ku, Fukuoka 819-0395, Japan

reported to exhibit mechanochromism,[32] but such examples are exceedingly rare and offer untapped potential for further exploration.

Recently, our group has focused on dinuclear triple-stranded helicates containing main-group elements as a new class of luminescent dyes.[33–38] Specifically, we have investigated aluminum-based helicates (ALPHY), which exhibit strong absorption and photoluminescence properties. Variations in the torsion angle of the ligand (–C═N–N═C–) can modulate the π-conjugation length, enabling multicolor emission. Taking advantage of the flexibility of the ALPHY skeleton, we hypothesized that changes in the aggregated solid state could induce variations in the torsion angle of the ligand, thereby inducing a mechanochromic response in the complex (Fig. 1(b)). To test this postulate, we synthesized a series of ALPHY derivatives and evaluated their optical properties in the solution, crystalline, and amorphous states.

In this study, we focus on derivatives exhibiting mechanochromism arising from the highly constrained torsion angles of the ligand in the crystalline state. During the course of this research, we discovered that these helicates exhibit reversible color and emission changes in response to grinding or treatment with solvents. We investigated this mechanochromic behavior in detail using single crystal X-ray structure diffraction (SCXRD), powder X-ray diffraction (PXRD), and optical property evaluations to understand the structure–property relationships. Although mechanochromism has been reported for aluminum complexes such as AlQ_3, the present study presents the first observation of mechanochromism in helical aluminum complexes and demonstrates a direct, reversible torsion-angle mechanism in such systems.

Results and discussion

We utilized a series of dinuclear aluminum-based triple-stranded helicates: **Me**, **H**, **Cl**, and **Br**, as shown in Fig. 2(a). Complexes **Me**, **H**, and **Br** were synthesized according to an established method,[34,36] whereas the synthesis of complex **Cl** was newly developed in this study. 4-Chloro-1H-pyrrole-2-carbaldehyde (**1**) was synthesized through the chlorination of pyrrole-2-carboxaldehyde using *N*-chlorosuccinimide in chloroform, with a yield of 27%. Compound **1** was then reacted with hydrazine monohydrate to produce compound $\mathbf{L_{Cl}}$ in 30%. Subsequently, compound **1** was reacted with aluminum chloride ($AlCl_3$) in the presence of triethylamine to obtain **Cl** in 28%. **Cl** was obtained as a racemic mixture of the (*M*)- and (*P*)-enantiomers, as discussed hereinafter. These new compounds were identified through nuclear magnetic resonance (NMR) and mass spectrometry analyses (Fig. S1–S7 and Tables S1–S2).

Optical measurements of the **Me**, **H**, **Cl**, and **Br** complexes were conducted in toluene solution. Absorption peaks were observed at 358, 390, 405, and 406 nm for **Me**, **H**, **Cl**, and **Br**, respectively, whereas the emission peaks appeared at 465 nm, 550 nm, 568 nm, and 566 nm, in the same order (Table 1, Fig. 3(a, c) and Fig. S8, S9, Tables S3, S4). All complexes exhibited large Stokes shifts, indicating minimal overlap between the absorption and emission spectra. This behavior has been reported previously and is attributed to significant structural relaxation of the ligand in the excited state.[37] The slight differences in the absorption and emission wavelengths of **H**, **Cl**, and **Br** complexes likely arise from changes in the electronic state of the ligand, induced by halogen substitution. In contrast, the absorption and emission wavelengths of the **Me** complex exhibited a pronounced blue-shift compared to those of the other complexes. This shift can be ascribed to steric hindrance induced by the methyl substituent at the methine position of ALPHY, which increases the ligand torsion angle of the ligands and consequently shortens the π-conjugation length. Consistent with this structural distortion, the **Me** complex showed a moderate photoluminescence quantum

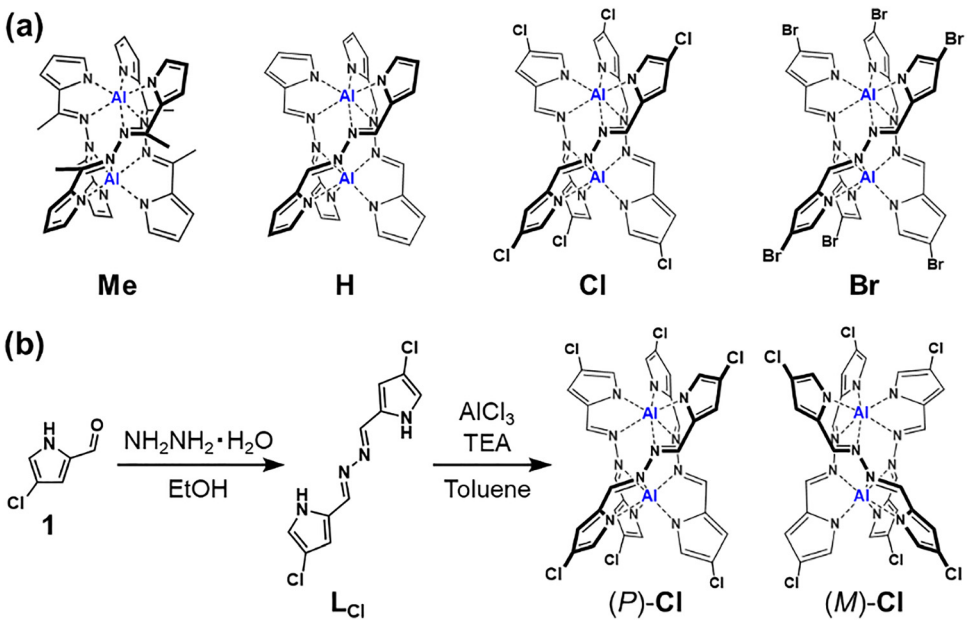

Fig. 2 (a) Chemical structures of **Me**, **H**, **Cl**, and **Br** complexes. Only (*P*)-isomer is shown. (b) Synthesis of (*P*)-**Cl** and (*M*)-**Cl**.

Table 1 Photophysical properties of all complexes in toluene and in the crystalline powder state at room temperature

	In toluene				In the solid state			
Compd.	$\lambda_{abs}^{max\,a}$ (nm)	$\lambda_{em}^{max\,b}$ (nm)	PLQY[cd]	τ_{av} (ns)	λ_{abs}^{max} [a] (nm)	λ_{em} [b] (nm)	PLQY[cd]	τ_{av} (ns)
Me	358	465	0.20	0.78	380	466	0.14	0.51
H	390	550	0.79	3.25	410	561	0.33	1.93
Cl	405	568	0.69	3.28	406	553	0.28	2.58
Br	406	566	0.29	2.12	408	568	0.11	1.11

[a] Absorption maxima. [b] Emission maxima. [c] Excited at λ_{abs}^{max}. [d] Absolute photoluminescence quantum yields.

yield (PLQY) of 20% in toluene. For comparison, the **H** and **Cl** complexes showed high PLQYs of 79% and 69%, respectively, whereas the **Br** complex exhibited a moderate PLQY of 29%. The reduced PLQY of the **Br** complex suggests that the heavy-atom effect of bromine promotes intersystem crossing from the excited singlet state to triplet state, resulting in non-radiative decay.[36] In contrast, the PLQY of the **Cl** complex was comparable to that of the **H** complex, indicating that the heavy atom effect of the chlorine atom does not influence the luminescence properties of the complex. Optical measurements of the **Me**, **H**, **Cl**, and **Br** complexes were carried out in the crystalline, powdered state (Table 1, Fig. 3(b, d) and Fig. S10, Table S5). The absorption and emission profiles of all complexes were similar to those observed in toluene. The emission maxima in the solid state appeared at 466, 561, 553, and 568 nm for **Me**, **H**, **Cl**, and **Br**, respectively; in addition, the PLQYs were 14%, 33%, 28%, and 11%, in the same order, demonstrating that these complexes act as efficient luminophores. The close similarity between the photoluminescence behaviors in solution and in the solid state suggests that the emission most likely originates from an intrinsic single-molecule excited state rather than from aggregation-induced emissive species. This result implies that

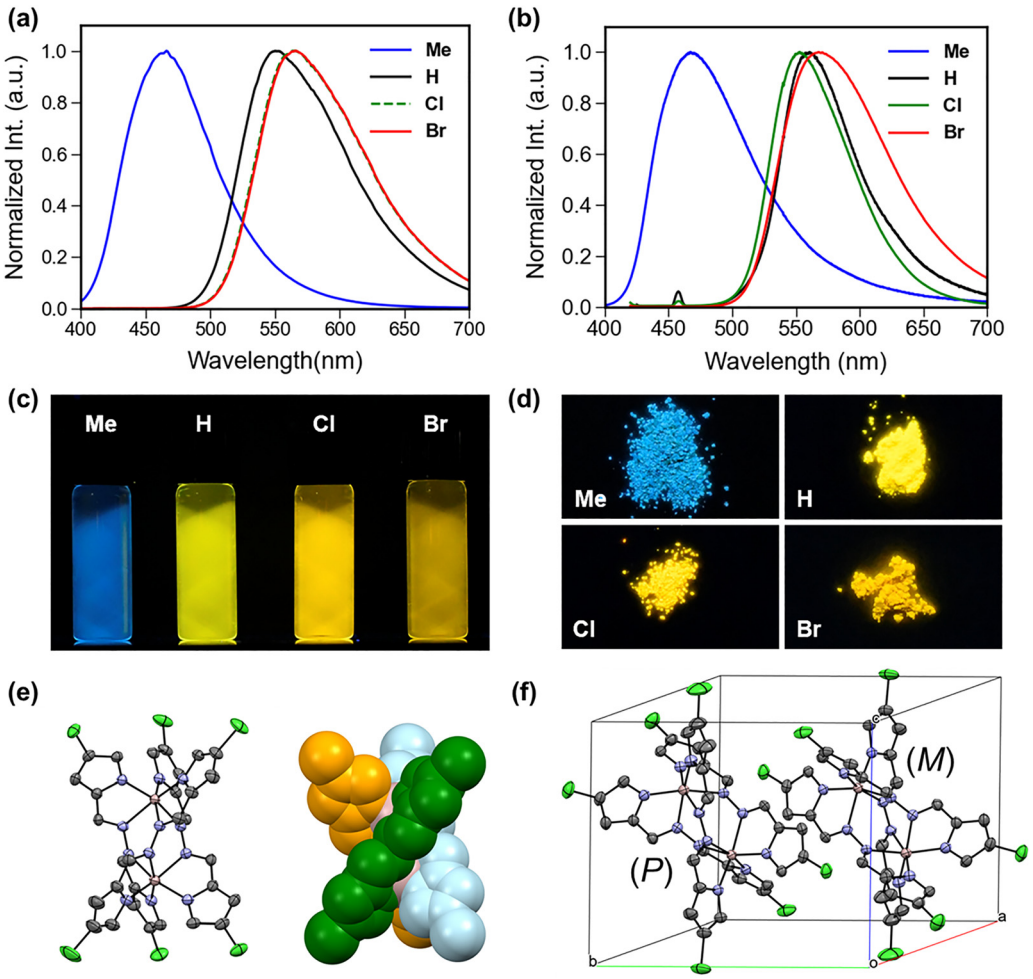

Fig. 3 (a) Emission spectra of **Me**, **H**, **Cl**, and **Br** complexes in toluene ($c = 10^{-6}$ M) and (b) in the crystalline powder state. The emission spectra were recorded upon excitation at the absorption maxima. (c) Photographs of the **Me**, **H**, **Cl**, and **Br** complexes in toluene solution and (d) in the crystalline powder state under UV irradiation at room temperature. (e) Crystal structures of **Cl**. The ellipsoid model represents a 50% probability; the space-filling model is shown on the right. The CCDC numbers are provided in the SI. In the structure depicted by using the ellipsoid model, carbon (C) atoms are represented in black, nitrogen (N) atoms in blue, aluminum (Al) atoms in pink, and chlorine (Cl) atoms in yellow-green. Hydrogen atoms are omitted for clarity. (f) Crystal packing of **Cl**, where the (*P*)- and (*M*)-enantiomers are identified.

intermolecular interactions in the solid state do not significantly affect the emission. This may be attributed to the three-dimensional (3D) molecular structure of the complexes, which appears to suppress strong packing effects such as π–π stacking. Consequently, the 3D framework allows the complexes to retain their inherent molecular-level emission in the solid state.

The **Me**, **H**, and **Br** complexes were crystallized from hexane–CH_2Cl_2 solutions, whereas the **Cl** complex was obtained from a hexane–THF solution. The single-crystal structures of the **Me**, **H**, **Cl**, and **Br** complexes are shown in Fig. 3(e, f) and Fig. S11. SCXRD analysis revealed that all four complexes formed racemic crystals comprising (*P*)- and (*M*)-enantiomers. The crystal structure of the **Me** complex contains no solvent molecules, whereas the **H**, **Cl**, and **Br** complexes appear to include solvent molecules originating from the recrystallization solvent. However, owing to severe disorder, these solvent molecules could not be assigned and the corresponding structures were refined using the solvent mask procedure.

The newly obtained **Cl** complex was separated into (*P*)- and (*M*)-enantiomers by chiral column chromatography. These enantiomers exhibited mirror-image circular dichroism (CD), and circularly polarized luminescence (CPL) spectra, with a $|g_{lum}|$ value of 0.003 at an emission wavelength of 550 nm in toluene, were obtained (for details, see Fig. S15–S21 and Tables S7–S12). However, because the amount obtained by optical resolution was insufficient for mechanochemical studies in the solid state, the subsequent experiments were conducted using the racemic form. The PXRD patterns of the bulk crystalline powders were consistent with those of the single crystal structures, indicating that the crystalline powders used in the

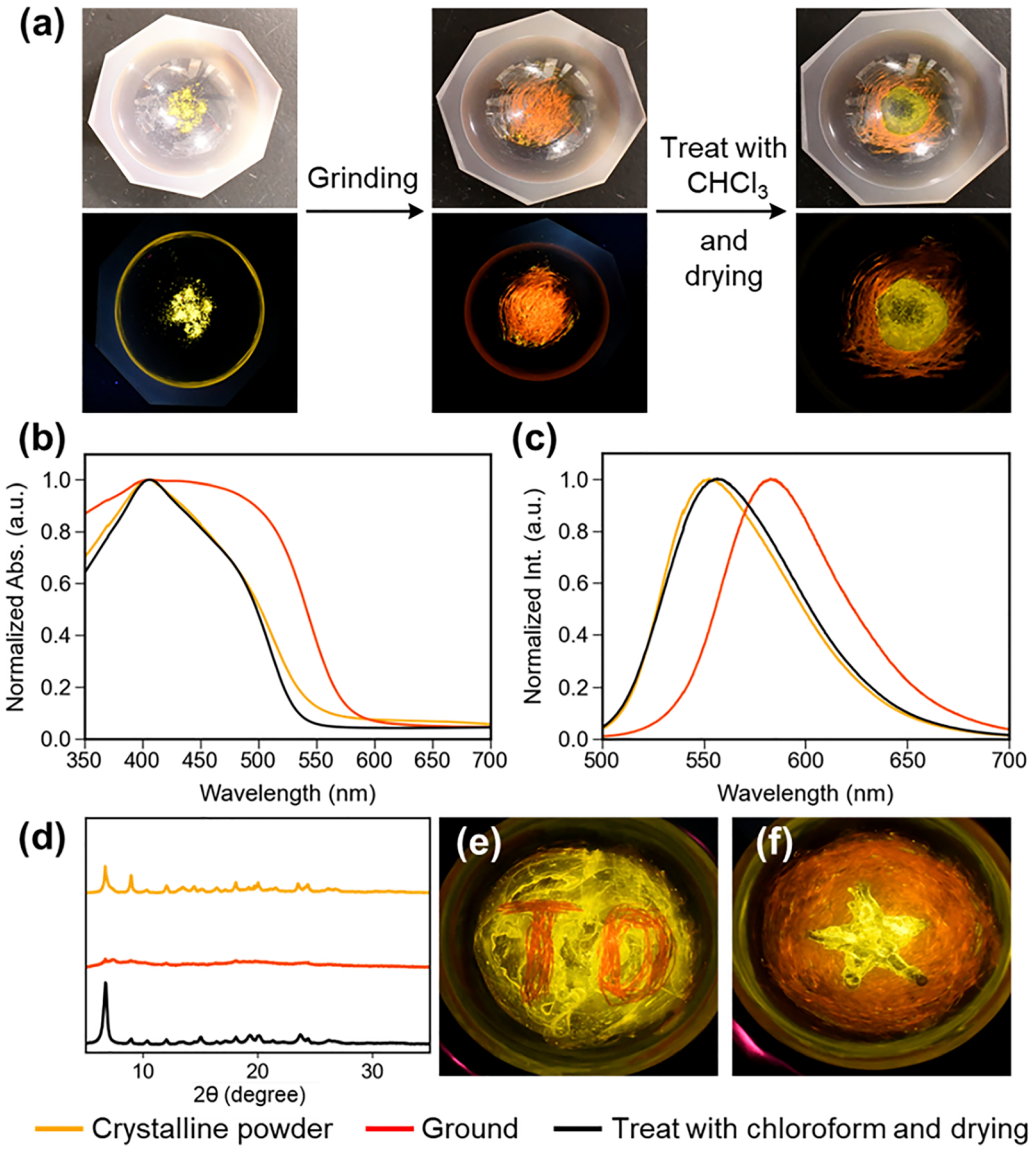

Fig. 4 (a) Photographs of the **Cl** complex under natural light and under UV irradiation before and after grinding. (b) Diffuse reflectance spectra, (c) emission spectra, and (d) PXRD patterns for the crystalline powder (black), ground (red) sample, and chloroform-treated and dried sample (orange). (e) and (f) Emission patterns of **Cl** under UV light, displaying the letters "TO" (e) and a star motif (f).

experiments retained the same packing structure as that of the single crystals (Fig. S12).

To investigate the mechanochromic properties, the crystalline samples were ground using an agate mortar and pestle, resulting in significant changes in both the coloration and emission color of the **H**, **Cl** and **Br** complexes (Fig. 4(a)–(c)). Specifically, grinding caused a change in the color of the samples from yellow to orange, accompanied by marked red shifts in the emission maxima: from 561 to 583 nm for **H**, from 553 to 578 nm for **Cl**, and from 568 to 599 nm for **Br**. Upon addition of chloroform to the ground powders followed by drying, the original emission color was restored. PXRD measurements revealed that grinding converted the crystalline samples into amorphous phases, which reverted to the crystalline states upon treatment with chloroform (Fig. 4(d)). Similar reversible behaviors were also observed upon addition of other organic solvents such as ethanol and ethyl acetate, or upon exposure to their vapors (Fig. S13). The slight differences in the emission color and intensity before and after grinding and solvent treatment are likely attributable to variations in the type of solvent molecules included in the crystals after recrystallization, which may cause subtle changes in the crystallinity. No emission color change occurred upon adding water to the ground samples, due to the low solubility of the complexes, indicating their stability toward water molecules. Furthermore, the absence of concentration dependence in both emission spectra and lifetimes (Fig. S14 and Table S6) suggests that intermolecular interactions, including excimer formation, are unlikely to play a significant role in the observed emission behavior.

In contrast, the **Me** complex did not exhibit mechanochromic properties upon grinding, most likely due to the steric hindrance from the methyl substituent at the methine moiety, which restricts changes in the torsion angles of the ligand. These results strongly suggest that the torsion angles of the ligand in the **H**, **Cl**, and **Br** complexes are effectively modulated by intermolecular interactions and molecular packing in the crystalline state (Fig. 5). The excellent mechanochromic properties of the **Cl** complex enabled the visualization of various letters and drawings. For instance, distinct patterns such as ‘‘TO’’ and even a ‘‘star’’ motif could be clearly observed (Fig. 4(e and f)). This demonstrates the potential of these aluminum-based functional dyes for diverse practical applications.

To obtain a deeper insight into the optical property modulation, we carried out time-resolved photoluminescence (TRPL) measurements for both crystalline and mechanically ground samples using a streak camera equipped with a polychromator. The crystalline sample exhibited a single time-resolved emission profile centered at 550 nm, with no detectable spectral evolution throughout the decay (Fig. 6(a)). This indicates a single emissive species with negligible inhomogeneity even in the solid state. In contrast, the ground sample displayed a red shift on a subnanosecond timescale after photoexcitation (Fig. 6(b)). Global analysis based on a two-component parallel model revealed at least two emissive species: a short-lived emission band with a time constant of 128 ps appearing around 560 nm and a longer-lived band with a time constant of 747 ps around 580 nm (Fig. S22). Because the emission energy of ALPHY derivatives is sensitive to the ligand conformation,[38] the two emission components observed in the ground sample might arise from different ligand torsion angles.

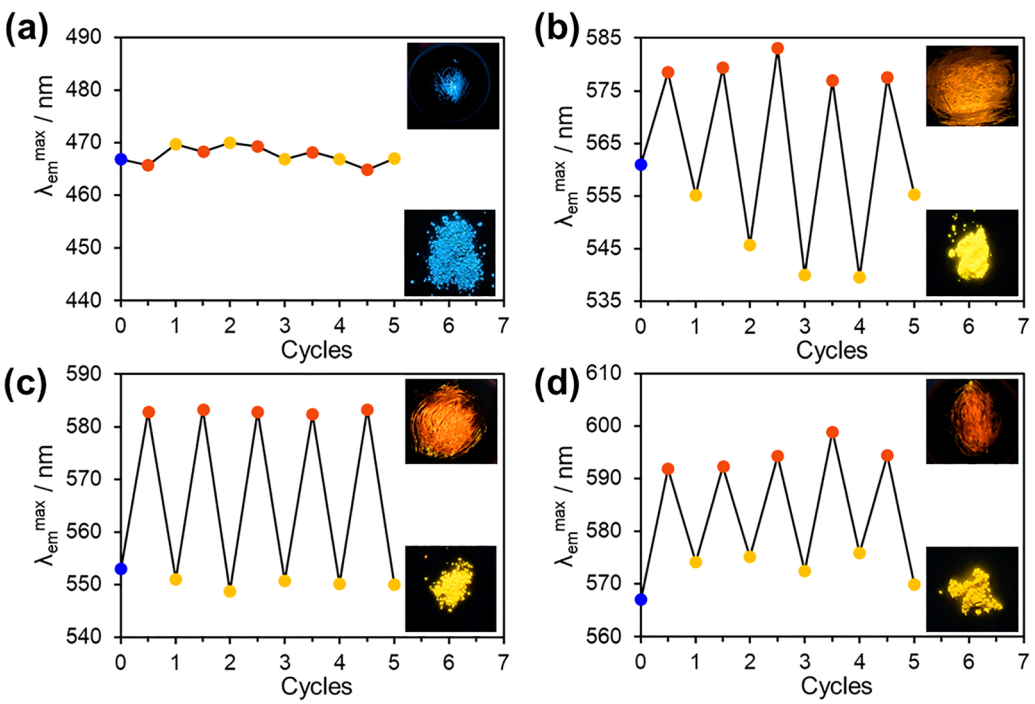

Fig. 5 Reversible switching of the emission maximum wavelength (λ_{em}^{max}) of (a) **Me**, (b) **H**, (c) **Cl** and (d) **Br** complexes during grinding–recovery cycles with chloroform.

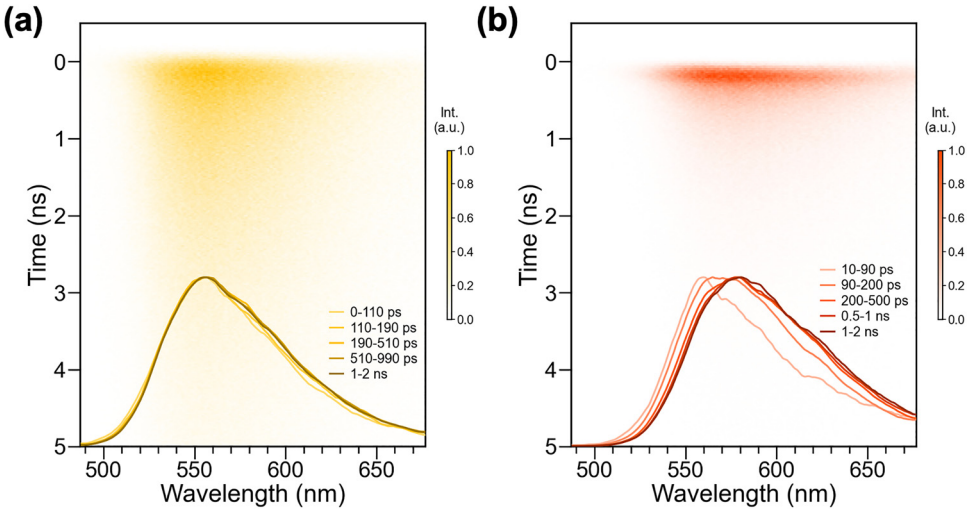

Fig. 6 Two-dimensional plots of TRPL spectra and the normalized spectral slices of the (a) crystalline powder and (b) ground states of **Cl**.

To gain a deeper understanding of the mechanochromic properties, we compared the torsion angles of the ligand (–C═N–N═C–) in the crystal structures with those in the most stable S_0 optimized (S_0 opt) geometries obtained from the DFT-based structures (Table 2). Note that the S_0 opt structures represent the lowest-energy configurations of the isolated molecules calculated using DFT *in vacuo* without considering intermolecular interactions or crystal packing effects. Although the ground state may not definitively correspond to the S_0 opt structure, the state after grinding, in which the intermolecular interactions are weakened, can be approximated using this structure. Indeed, for the **Cl** complex, it is inferred that the torsion angle of the ligand in the crystalline state (85°) may approach the S_0 opt-calculated value of 69° upon grinding. This reduction in the torsion angle plausibly extended the π-conjugation, resulting in a red-shift of the absorption and emission color from yellow to orange. In contrast, for the **Me** complex, the torsion angle of the ligand is estimated to change only slightly (from 94° in the crystalline state to approximately 91° in the S_0 opt structure), suggesting minimal structural alteration upon grinding. Because the torsion angle of the ligand remained nearly unchanged even after grinding and solvent treatment, the π-conjugation length was not significantly altered, which likely accounts for the minimal change in the emission color.

Finally, time-dependent density functional theory (TD-DFT) calculations were performed to compliment the spectroscopic analysis. Specifically, the torsion angle of the ligand was fixed at 69°, 75°, and 85°, and geometry optimizations were carried out for each configuration. The absorption spectra were then simulated at the CAM-B3LYP/6-31G(d,p) level of theory. An apparent blue-shift in the absorption spectra was observed with increasing torsion angles (Fig. S23 and Tables S13–S15), indicating that increasing the torsion angle of the ligand shortens the π-conjugation, thereby suppressing electronic delocalization throughout the molecule and causing the absorption band to shift to higher energy. These calculations thus provide theoretical support proving that torsional deformation of the ligand directly modulates the optical properties of the complex.

Table 2 Ligand torsion angles of the –C═N–N═C– moiety for **Me** and **Cl** complexes obtained from single-crystal structures and DFT optimized structures

Compd.		Al–Al distance (Å)	–C═N–N═C– torsion angle (deg)		
Me	Crystal	3.882	93.1	93.4	95.6
	S_0 opt	3.843	91.2	91.3	91.3
Cl	Crystal	3.876	83.4	85.1	85.8
	S_0 opt	3.859	69.0	69.0	69.2

Conclusions

In summary, this study provides a detailed evaluation of the mechanochromic properties of dinuclear aluminum-based triple-stranded helicates. Optical measurements and powder X-ray diffraction analysis revealed that the **Cl** complex, in particular, exhibits significant color and emission changes upon grinding, together with reversible recovery of the original emission upon treatment with chloroform. Comparison of the torsion angles of the ligand in the crystalline state with those obtained from DFT calculations strongly suggests that the torsion angle of the ligand is larger in the crystalline state and decreases upon amorphization induced by grinding. This reduction in the torsion angle alters the π-conjugation, leading to a change in the emission color. Although helicates have been known for several decades and research has primarily focused on constructing and understanding their structures,[39–41] most luminescent examples rely on lanthanide-based metal ions,[42,43] whereas reports on ligand-centered emission are exceedingly rare; aside from a few zinc complexes,[44,45] such examples are virtually nonexistent. The present results reveal mechanochromism arising from reversible changes in the ligand torsion angle in dinuclear triple-stranded helical aluminum complexes.

These findings provide new insights into the mechanism of mechanochromism in aluminum complexes and highlight the potential of luminescent aluminum helicates as responsive functional materials. The results represent an important step toward the design of responsive functional materials based on luminescent aluminum complexes, with promising implications for next-generation optical devices and sensor applications. Although racemic samples were used in this study, we are currently investigating the external stimulus responsiveness of enantiomerically pure complexes obtained by optical resolution.

Author contributions

T. O. supervised the overall concept of the study and the preparation of the manuscript and also performed the computational chemistry studies. T. U. performed most of the synthetic experiments and photophysical measurements. A. T. conducted the experiments related to mechanochromism. Y. K. contributed to the synthetic experiments and part of the computational chemistry studies. Y. I. carried out single-crystal preparation and structural analysis. T. H. performed circularly polarized luminescence measurements. T. E. and K. M. conducted time-resolved photoluminescence spectroscopy measurements. K. O. and Y. H. contributed through helpful discussions on the experimental results. All authors have approved the final version of the manuscript.

Conflicts of interest

The authors declare no conflicts of interest.

Data availability

The data supporting this article have been included as part of the supplementary information (SI). Supplementary information: experimental procedures, characterization data of the compounds (NMR and MS), crystallographic data, optical properties (UV-vis, emission, lifetime, PLQY, CD, and CPL), and computational details (PDF). See DOI: https://doi.org/10.1039/d5tc04488j.

CCDC 2497171 and 2497172 contain the supplementary crystallographic data for this paper.[46a,b]

Acknowledgements

This work was supported by JSPS KAKENHI Grant Numbers (JP24K01471, JP23K04815, JP25K22276, JP25H00873, JP24KK0256, JP25KJ1949, JP23H01977, JP23K20039, JP25H01678, JP24K01515, and JP23H03833). We would like to express our gratitude for the support received from the Asahi Glass Foundation, the Tokuyama Science Foundation, the Mazda Foundation, and the Nissan Chemical Corporation. Additional support was provided by the Kyushu University Platform of Inter-/Transdisciplinary Energy Research (Q-PIT), including its Module-Research Program. Furthermore, this study was supported by the Data Creation and Utilization-Type Material Research and Development Project (Grant number JPMXP1122714694). Computational resources were provided by the Research Institute for Information Technology, Kyushu University, under the general projects category.

References

1 Z. Chi, X. Zhang, B. Xu, X. Zhou, C. Ma, Y. Zhang, S. Liu and J. Xu, *Chem. Soc. Rev.*, 2012, **41**, 3878–3896.
2 X. Zhang, Z. Chi, Y. Zhang, S. Liu and J. Xu, *J. Mater. Chem. C*, 2013, **1**, 3376–3390.
3 P. Xue, J. Ding, P. Wang and R. Lu, *J. Mater. Chem. C*, 2016, **4**, 6688–6706.
4 M. Kato, H. Ito, M. Hasegawa and K. Ishii, *Chem. – Eur. J.*, 2019, **25**, 5105–5112.
5 S. Ito, *Chem. Lett.*, 2020, **50**, 649–660.
6 S. Ito, *J. Photochem. Photobiol., C*, 2022, **51**, 100481.
7 F. Khan, A. Ekbote, G. Singh and R. Misra, *J. Mater. Chem. C*, 2022, **10**, 5024–5064.
8 Y. Hirai, *ACS Appl. Opt. Mater.*, 2024, **2**, 1025–1045.
9 Y. Sagara, T. Mutai, I. Yoshikawa and K. Araki, *J. Am. Chem. Soc.*, 2007, **129**, 1520–1521.
10 T. Butler, W. A. Morris, J. Samonina-Kosicka and C. L. Fraser, *ACS Appl. Mater. Interfaces*, 2016, **8**, 1242–1251.
11 Y. Tani, M. Terasaki, M. Komura and T. Ogawa, *J. Mater. Chem. C*, 2019, **7**, 11926–11931.
12 K. Sugawara, T. Ono, Y. Yano, T. Suzuki and Y. Ishigaki, *Mater. Chem. Front.*, 2023, **7**, 1591–1598.
13 K. Noro, A. Tani, T. Tadokoro, T. Harimoto, K. Sugawara, T. Suzuki, T. Ono and Y. Ishigaki, *J. Org. Chem.*, 2025, **90**, 12727–12733.
14 A. Tani, L. Cui, R. Furuta, Y. Hoshino and T. Ono, *ACS Appl. Opt. Mater.*, 2025, **3**, 1287–1296.
15 Y. Sagara, S. Yamane, M. Mitani, C. Weder and T. Kato, *Adv. Mater.*, 2016, **28**, 1073–1095.
16 K. Imato and Y. Ooyama, *Macromol. Chem. Phys.*, 2023, **224**, 2300316.
17 T. Ono, Y. Tsukiyama, A. Taema, H. Sato, H. Kiyooka, Y. Yamaguchi, A. Nagahashi, M. Nishiyama, Y. Akahama, Y. Ozawa, M. Abe and Y. Hisaeda, *ChemPhotoChem*, 2018, **2**, 416–420.
18 S. Irii, T. Ogaki, H. Miyashita, K. Nobori, Y. Ozawa, M. Abe, H. Sato, E. Ohta, Y. Matsui and H. Ikeda, *Tetrahedron Lett.*, 2022, **101**, 153913.
19 M. Yoshida and M. Kato, *Coord. Chem. Rev.*, 2018, **355**, 101–115.
20 C.-J. Lin, Y.-H. Liu, S.-M. Peng, T. Shinmyozu and J.-S. Yang, *Inorg. Chem.*, 2017, **56**, 4978–4989.
21 M. Yoshida, V. Sääsk, D. Saito, N. Yoshimura, J. Takayama, S. Hiura, A. Murayama, K. Põhako-Esko, A. Kobayashi and M. Kato, *Adv. Opt. Mater.*, 2022, **10**, 2102614.
22 T. Seki and A. Yano, *Eur. J. Inorg. Chem.*, 2025, e202400793.
23 S. Cheng, Z. Chen, Y. Yin, Y. Sun and S. Liu, *Chin. Chem. Lett.*, 2021, **32**, 3718–3732.

24 H. Ito, T. Saito, N. Oshima, N. Kitamura, S. Ishizaka, Y. Hinatsu, M. Wakeshima, M. Kato, K. Tsuge and M. Sawamura, *J. Am. Chem. Soc.*, 2008, **130**, 10044–10045.
25 H. Ito, M. Muromoto, S. Kurenuma, S. Ishizaka, N. Kitamura, H. Sato and T. Seki, *Nat. Commun.*, 2013, **4**, 2009.
26 T. Seki, Y. Takamatsu and H. Ito, *J. Am. Chem. Soc.*, 2016, **138**, 6252–6260.
27 S. Li, M. Wu, Y. Kang, H.-W. Zheng, X.-J. Zheng, D.-C. Fang and L.-P. Jin, *Inorg. Chem.*, 2019, **58**, 4626–4633.
28 X. Yan, X. Song, X. Mu and Y. Wang, *New J. Chem.*, 2019, **43**, 15886–15891.
29 C. Li, W. Li, A. F. Henwood, D. Hall, D. B. Cordes, A. M. Z. Slawin, V. Lemaur, Y. Olivier, I. D. W. Samuel and E. Zysman-Colman, *Inorg. Chem.*, 2020, **59**, 14772–14784.
30 R. Zhang, J.-W. Liu, W.-Y. Zhong, J.-L. Chen, F. Zhao, S.-J. Liu and H.-R. Wen, *Inorg. Chem.*, 2023, **62**, 11510–11517.
31 A. Gusev, E. Braga, E. Zamnius, M. Kiskin, A. Ali, G. Baryshnikov and W. Linert, *Dalton Trans.*, 2023, **52**, 14995–15008.
32 H. Bi, D. Chen, D. Li, Y. Yuan, D. Xia, Z. Zhang, H. Zhang and Y. Wang, *Chem. Commun.*, 2011, **47**, 4135–4137.
33 T. Ono and Y. Ooyama, *Dalton Trans.*, 2025, **54**, 6361–6368.
34 T. Ono, K. Ishihama, A. Taema, T. Harada, K. Furusho, M. Hasegawa, Y. Nojima, M. Abe and Y. Hisaeda, *Angew. Chem. Int. Ed.*, 2021, **60**, 2614–2618.
35 K. Ishihama, T. Ono, T. Okawara, T. Harada, K. Furusho, M. Hasegawa, Y. Nojima, T. Koide, M. Abe and Y. Hisaeda, *Bull. Chem. Soc. Japan*, 2021, **94**, 573–578.
36 Y. Konishi, T. Ehara, L. Cui, K. Ueno, Y. Ishigaki, T. Harada, T. Konta, K. Onda, Y. Hoshino, K. Miyata and T. Ono, *Inorg. Chem.*, 2024, **63**, 11716–11725.
37 K. Ueno, Y. Konishi, L. Cui, T. Harada, K. Ishibashi, T. Konta, A. Muranaka, Y. Hisaeda, Y. Hoshino and T. Ono, *Inorg. Chem.*, 2024, **64**, 6296–6304.
38 T. Ehara, Y. Yoneda, T. Yoshida, T. Ogawa, Y. Konishi, T. Ono, A. Muranaka, H. Kuramochi, K. Miyata and K. Onda, *J. Am. Chem. Soc.*, 2025, **147**, 26446–26455.
39 J. M. Lehn, A. Rigault, J. Siegel, J. Harrowfield, B. Chevrier and D. Moras, *Proc. Natl. Acad. Sci. U. S. A.*, 1987, **84**, 2565–2569.
40 C. Piguet, G. Bernardinelli and G. Hopfgartner, *Chem. Rev.*, 1997, **97**, 2005–2062.
41 M. Albrecht, *Eur. J. Inorg. Chem.*, 2020, 2227–2237.
42 Y. B. Tan, Y. Okayasu, S. Katao, Y. Nishikawa, F. Asanoma, M. Yamada, J. Yuasa and T. Kawai, *J. Am. Chem. Soc.*, 2020, **142**, 17653–17661.
43 M. Hasegawa and H. Ohmagari, *Chem. Lett.*, 2020, **49**, 845–854.
44 T. E. Wood, N. D. Dalgleish, E. D. Power, A. Thompson, X. Chen and Y. Okamoto, *J. Am. Chem. Soc.*, 2005, **127**, 5740–5741.
45 T. E. Wood, A. C. Ross, N. D. Dalgleish, E. D. Power, A. Thompson, X. Chen and Y. Okamoto, *J. Org. Chem.*, 2005, **70**, 9967–9974.
46 (*a*) CCDC 2497171: Experimental Crystal Structure Determination, 2026, DOI: 10.5517/ccdc.csd.cc2pthxy; (*b*) CCDC 2497172: Experimental Crystal Structure Determination, 2026, DOI: 10.5517/ccdc.csd.cc2pthyz.

